Locally Auxetic Behavior of Elastomeric Polypropylene on the 100 nm Length Scale

Mechthild Franke* and Robert Magerle*

Fakultät für Naturwissenschaften, Technische Universität Chemnitz, 09107 Chemnitz, Germany

ABSTRACT We observe unexpected locally auxetic behavior in elastomeric polypropylene, a semicrystalline polymer with a natural microstructure and a low degree of crystallinity. Our series of scanning force microscopy images show the nanomechanical deformation processes that occur upon stretching a thin film of elastomeric polypropylene. Upon uniaxial stretching, the angle between epitaxially grown lamella branches remains constant and the lamellae elongate, resulting in locally auxetic behavior (negative Poisson's ratio) on the 100-nanometer scale. This mechanism causing auxetic behavior, which was previously proposed on the basis of geometric arguments, appears to be an intrinsic property of certain semicrystalline polymers.

KEYWORDS: negative Poisson's ratio · nanomechanics · semicrystalline polymers · thin films · scanning force microscopy

Auxetic materials are materials with a negative Poisson's ratio; they expand laterally when stretched. This unusual behavior was originally attributed to a microstructure forming a reentrant network.[1−3] Meanwhile, additional mechanisms causing auxetic behavior and materials with corresponding microstructures on molecular as well as macroscopic length scales have been found,[4−6] such as certain molecular networks,[3,7−9] networks of dilating elastic elements,[10−12] expanding chiral honeycomb lattices,[13,14] and rotating rigid units.[15−17] Nevertheless, auxetic materials rarely occur naturally. Particular processing steps are required for producing polymeric materials with auxetic behavior such as foams,[1,18,19] microporous films and fibers,[20−24] and macroscopically perforated sheets.[25,26] Among the large class of semicrystalline polymers with a natural microstructure, auxetic behavior has not been previously found. In these intrinsically nanostructured materials, 10 nm thick crystalline lamellae strengthen the material and act as physical cross-links for the polymer molecules. The spatial arrangement and mechanical stability of crystalline regions are important factors in determining the mechanical properties of the material.[27] Previous micromechanical studies focused on averaged crystal orientation,[28−37] crystallinity during straining,[34,36] and the study of crazing,[38,39] which is a common failure mechanism of these materials. Here, we report on unexpected locally auxetic behavior in elastomeric polypropylene (ePP), a semicrystalline polymer with a low degree of crystallinity.[40] Our results reveal a mechanism for auxetic behavior similar to the stretching mechanism proposed by Rothenburg *et al.*[10] based on purely geometric arguments. Its manifestation in ePP is related to the intrinsic properties of the material on the nanometer scale.

RESULTS AND DISCUSSION

Figure 1a shows a scanning force microscopy (SFM) phase image of the surface of an ~1 μm thick film of ePP before stretching. The 10 nm thick crystalline lamellae appear as bright lines because they are oriented perpendicular to the film surface.[41] The polymer forms long mother lamellae on which short epitaxial branches grow, forming an angle of 80° between the mother and daughter lamellae.[42−44] The lamellae are straight before the film is stretched (Figure 1a). Upon stretching the film in the *y*-direction to ε = 40% (Figure 1b), the lamellae deform in various ways: some buckle, others bend, and others break up into smaller fragments. The deformations are not affine on the submicrometer scale. On larger length scales (>1 μm), the deformations follow the uniaxial stretching with negligible lateral contraction as given by the slit geometry. We compiled the series of SFM phase images during stretching into an animated image sequence (see Supporting Information), which gives an impression of the deformations that occur on the 100 nm scale as the film is stretched. Connection points between large clusters of lamellae become obvious as well as clusters of lamellae moving

* Address correspondence to mechthild.franke@physik.tu-chemnitz.de, robert.magerle@physik.tu-chemnitz.de.

Received for review September 23, 2010 and accepted April 15, 2011.

Published online April 15, 2011
10.1021/nn200957g

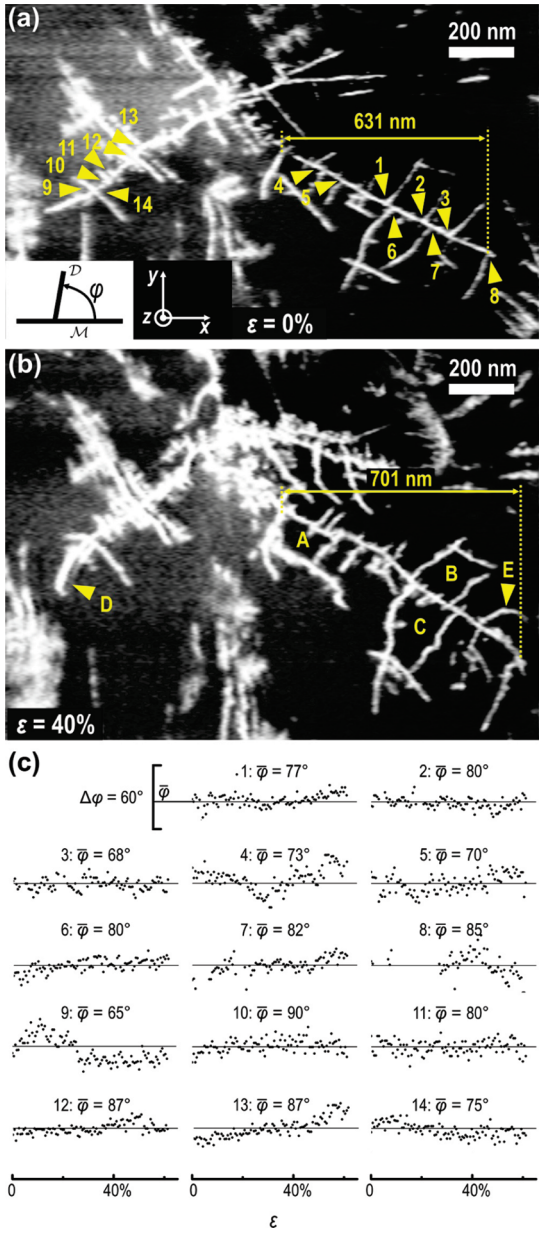

Figure 1. SFM phase images of an ePP film before (a) and after stretching the film in the *y*-direction to a global strain of $\varepsilon = 40\%$ (b). Quadrilaterals A, B, and C are shown in Figure 2. D and E mark bending lamellae. (c) Angle φ between mother ($\mathcal{M}$) and daughter lamella ($\mathcal{D}$) as function of global strain ε. For the branching numbered in (a) the average angle $\bar{\varphi}$ over the interval from $\varepsilon = 0\%$ to $\varepsilon = 40\%$ is given and indicated with a solid line. The φ-scale is the same for all angles.

independently from each other. The deformation behavior of the crystal complex shown in Figure 1a and b resembles a tree branch that is pulled through a highly viscous liquid. This is plausible since the crystals are solid with a Young's modulus of 40 GPa along the chain direction,[45] and the amorphous matrix is viscoelastic at room temperature.[40,46,47] Furthermore, this mother lamella widens perpendicular to the stretching direction from 631 nm at ε = 0% to 701 nm at ε = 40%.

We now address the deformation behavior of individual crystalline lamellae and their branchings displaying locally auxetic behavior on the 100 nm length scale. A striking feature is that the acute angles formed between mother and daughter lamellae remain unchanged up to global strains of $\varepsilon = 40\%$ (Figure 1c). The scatter corresponds to the accuracy of the measurement. The mean values are ~80°, in accordance with the epitaxial growth mechanism.[42−44] At strains larger than ε = 40%, some angles widen by ~10° to 20°.

Figure 2 shows SFM phase images of lamellae that are arranged in such a way that they form irregular quadrilaterals with one diagonal oriented roughly along the stretching direction with sizes from ~100 nm (Figure 2a−c) to ~1 μm (Figure 2d). The lamellae elongate up to 1.5 times their initial length (Figure 2). This large relative elongation of up to 50% is unexpected considering that deformations of crystalline lattices upon straining are on the order of only a few percent.[48] On the 100 nm length scale, the quadrilaterals widen along the stretching direction as well as perpendicular to it. On the macroscopic scale, the deformation of a material perpendicular to the strain direction is described by Poisson's ratio. In analogy to this concept, we describe the deformation behavior of individual quadrilaterals by a local Poisson's ratio, $\nu = -(\Delta d/d)/(\Delta l/l)$, where d and l are the width and length of the quadrilateral perpendicular and parallel to the stretching direction of the film, respectively, and Δd and Δl are the corresponding changes. ν = −0.68, −2.59, and 0.18 at ε = 60% for the cases shown in Figure 2a, b, c, respectively. On the 1 μm scale, the quadrilateral shown in Figure 2d elongates only along the stretching direction and keeps its width perpendicular to the stretching direction, corresponding to a local Poisson's ratio of ν = 0.0072.

Also the right-hand branch of the crystal complex shown in Figure 1a widens perpendicularly to the stretching direction from 631 nm at ε = 0% to 701 nm at ε = 40%. A local widening perpendicular to the stretching direction is also visible in other regions of the film (see Supporting Information). Almost all the lamellae elongate. Furthermore, there is no correlation between the relative elongation of a lamella and the fact that a lamella is a mother or daughter lamella.

In addition to the lamella length, we measured the angles of the quadrilaterals during stretching. The angles of the ~100 nm large quadrilaterals change by less than 10° for ε < 40% (Figure 2a−c), whereas those of the 1 μm large quadrilateral change up to 40° (Figure 2d). On the basis of the results of the deformation behavior of the angles between mother and daughter lamella (Figure 1), we conclude that angles that do not or only slightly deform are formed by epitaxially grown daughter lamellae; angles that change significantly are unlikely to be formed by

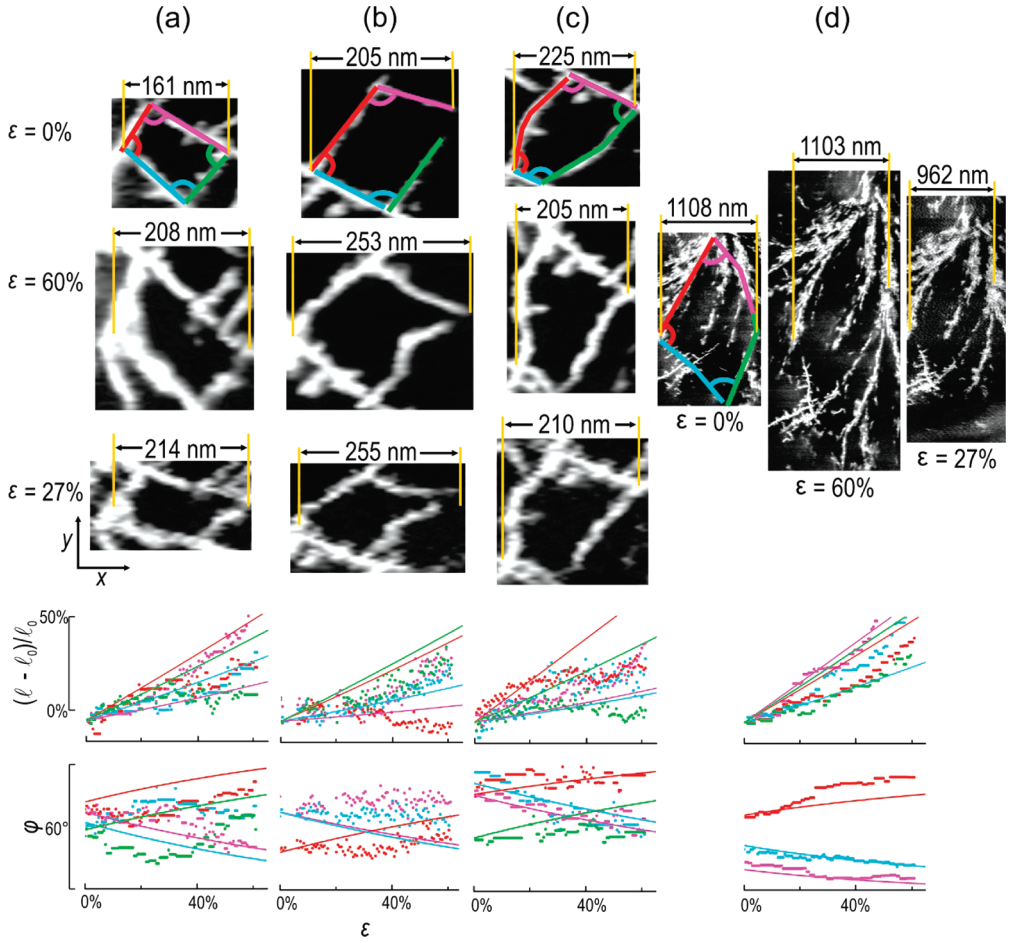

Figure 2. Deformation behavior of individual crystal complexes: (a–c) on the 100 nm scale, (d) on the 1 μm scale. SFM phase images at ε = 0%, ε = 60%, and after releasing the strain to ε = 27%, relative elongation of crystalline lamellae marked in the SFM images, and angles between these crystalline lamellae as a function of global strain ε (from top to bottom). The colors in the SFM images correspond to the colors of the data points. The lines show the expected behavior assuming no expansion of the quadrilaterals in the *x*-direction.

epitaxially grown daughter lamellae. The deformation behavior of quadrilaterals that do not deform perpendicular to the stretching direction can be directly derived from geometric relations (see the Materials and Methods section) and is shown as solid lines in Figure 2. The assumption of no deformations perpendicular to the stretching direction is motivated by the global constraints imposed on the film by the slit geometry. The model describes the trend and the magnitude of the measured relative lamella elongations for $\varepsilon < 30\%$ as well as the change of angles for the quadrilaterals with a local Poisson's ratio ν = 0.18 (Figure 2c) and 0.0072 (Figure 2d). However, the model fails for the quadrilaterals with a negative local Poisson's ratio (Figure 2a,b). It predicts a change of angles with increasing global strain ε. In contrast to this, the measured angles are constant for $\varepsilon < 40\%$, as is also observed for other angles between mother and daughter lamellae (Figure 1). The local Poisson's ratio of the quadrilateral shown in Figure 2b is $\nu = -2.59$. This value is smaller than -1, which indicates that this quadrilateral widens more than it elongates. A behavior where

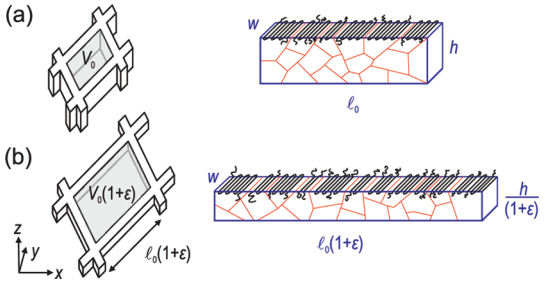

Figure 3. Sketches of the assumed deformation behavior of a quadrilateral of crystalline lamellae (left) and an individual crystalline lamella forming one side of the quadrilateral (right, viewed perpendicular to the lamella side) upon stretching the ePP film along the *y*-direction. The grain structure of the lamella is indicated. (a) Initial state, (b) after deformation. The lamella width *w* is constant. The volume *V* of the amorphous region enclosed by a quadrilateral is marked in gray. It increases upon stretching the film: $V = V_0(1 + \varepsilon)$.

only the sides of the quadrilateral elongate while the angles stay constant corresponds to a local Poisson's ratio of $\nu = -1$. On releasing the strain, the quadrilaterals shrink along the stretching direction. In contrast,

their widths remain almost constant perpendicular to the stretching direction. This is accompanied by a shortening of the lamellae and changes of the angles of the quadrilaterals (Figure 2). Since the maximum global strain of $\varepsilon = 61\%$ is beyond the elastic limit of the material,[20] we attribute the relaxation behavior to partially plastic deformations of the microstructure.

We now discuss possible explanations of the observed deformation behavior during stretching. We observe that many crystalline lamellae break into smaller fragments, which supports the models of Strobl[49] and Sirota,[50] who proposed that each lamella is a mosaic of ~10 nm large crystalline grains. Other lamellae, in particular those forming the large crystal complex shown in Figure 1 and the ~100 nm large quadrilateral shown in Figure 2a–c, elongate considerably while retaining their continuous shape even at large global strain. The elongation is an order of magnitude larger than the elongation of the lattice constant during straining.[48] The apparent growth during straining can be explained with the block model of crystalline lamellae.[49,50] One explanation is that the growth of the lamellae occurs at the grain boundaries between the small grains when they are pulled apart. An alternative explanation is a rearrangement of grains *via* motion of grain boundaries within a lamella (Figure 3). On length scales $\geq 1\ \mu$m no deformations occur along the *x*-direction (Figure 2d). This is in accordance with the global constraints imposed on the film by the slit geometry. This fact and the assumption that the volume is conserved on length scales $\geq 1\ \mu$m imply that the thickness *h* of the film is reduced to $h/(1+\varepsilon)$ upon stretching the polymer film. We will show that this is an important factor causing the locally auxetic behavior. For $\varepsilon = 60\%$, the film thickness should decrease by 37.5%. This is corroborated by an observed decrease of the height corrugation of the film surface. We can only speculate about the internal rearrangements of the crystalline lamellae during this change of shape. Lamellae are oriented perpendicular to the film surface and are known to extend throughout the entire film.[41] Since we do not observe individual lamellae poking out of the film surface upon stretching the film, we assume that the height of each lamella is reduced by the factor $(1+\varepsilon)^{-1}$ (Figure 3). This decrease in lamella height is accompanied by the apparent growth of the crystalline region along the long axis of the lamella so as to conserve the volume of crystalline material within each lamella since the width of lamellae are known not to change during straining.[29] The entanglements of polymer chains prevent the increase of the lamella width during deformations. This is the same reason that limits the growth of lamella width during crystallization.[49] The local conservation of the volume of the crystalline material implies that the overall crystallinity of the sample does not change during straining. This agrees with observations that more than 300% strain is required for inducing additional crystallization of this material.[34]

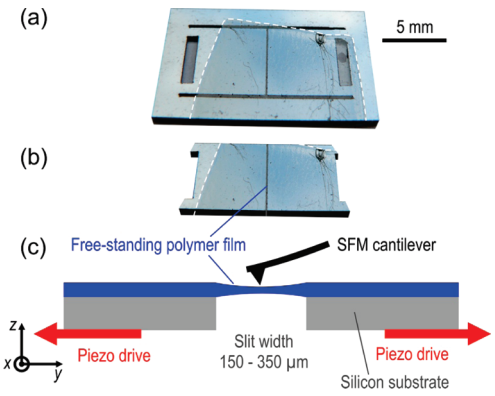

Figure 4. Schematic diagram of the setup used in the micromechanics experiment. (a) Silicon substrate with a support frame and a polymer film (marked by a dashed line) deposited across the slit. The slotted substrate was cut from a silicon wafer with a water-jet-guided laser (Laser MicroJet, SYNOVA, Lausanne, Switzerland). (b) The substrate with the free-standing film is glued onto a piezoelectric-driven symmetric stretching device (d-Drive, Piezosystem Jena, Jena, Germany), and after the glue has hardened, the support frame is removed. (c) The free-standing polymer film is stretched and its microstructure is observed with SFM at the surface of the film. The movement of the piezo drive was calibrated using an optical microscope.

The proposed deformation mechanism of quadrilaterals implies that the volume *V* of the amorphous region enclosed by a quadrilateral increases by the factor $(1+\varepsilon)$ upon stretching the polymer film in the *y*-direction. The dilation of the volume *V* enclosed by a quadrilateral validates identifying this deformation behavior as locally auxetic deformation behavior. Furthermore, if the number of atoms within the volume $V = V_0(1+\varepsilon)$ does not change, the increase in volume corresponds to a reduction of the density by a factor $(1+\varepsilon)^{-1}$. This local density decrease is probably accompanied by a compression of the amorphous regions surrounding the expanding quadrilateral. Due to this micromechanical deformation mechanism, spatial density heterogeneities are expected to be generated on the 100 nm length scale upon stretching the polymer film. Since we do not observe a depression of the film surface inside the quadrilaterals or a squeeze-out of amorphous material in the vicinity of those quadrilaterals, we conclude that if such density heterogeneities are initially created by stretching the film, they relax within the time required to measure the SFM images (within an hour or more). This time is much larger than the time constant of stress relaxation in ePP, which ranges between 10 s and 30 min.[46,47] Some very interesting and open questions in this context are the roles of molecular conformations within the amorphous phase, the topology of the network formed by the entanglements and polymer chains anchored in the crystalline regions, and the deformations of the molecular network upon stretching the film.

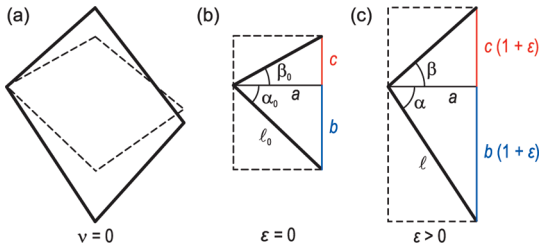

Figure 5. (a) In-plane deformation of a quadrilateral upon uniaxial elongation along one of its diagonals. In the perpendicular direction, the quadilateral's width does not change. The sides elongate and the angles change upon this uniaxial elongation. (b) Left-hand side of the quadrilateral at $\varepsilon = 0$ and (c) at $\varepsilon > 0$.

Large-scale computer simulations based on molecular dynamics and/or Monte Carlo methods are required to resolve these questions.

CONCLUSIONS

The constant width of the crystalline lamellae and the volume conservation of crystalline material cause the elongation of lamellae along their long axis. The epitaxial relationship between mother and daughter lamellae explains the mechanical stability of their connection during straining. As a result, the increase in length combined with the fixed angles between mother and daughter lamellae cause the locally auxetic behavior on the 100 nm length scale. This is a manifestation of the general, length-scale-independent mechanism for auxetic behavior that was proposed by Rothenburg *et al.*[10] based on purely geometric arguments. Our results show that locally auxetic behavior is an intrinsic property of certain semicrystalline polymers. More broadly, our results demonstrate that a microstructure configuration of elements that only elongate upon straining while maintaining constant angles between them is a feasible route for the design of auxetic materials. An example of such a material might be α-polypropylene, where crystalline lamellae form a cross-hatch structure,[43,44] which is a continuous network of ∼100 nm large quadrilaterals, like that in our work.

MATERIALS AND METHODS

We developed a sample preparation technique and a tensile straining setup that allow the deformations of individual crystalline lamellae at increasing degrees of strain to be imaged with scanning force microscopy. We investigated elastomeric stereoblock polypropylene polymerized by metallocene catalysis[40] with a weight-average molecular weight of 153 kg/mol, an [mmmm] pentad content of 26%, which corresponds to 12% crystallinity,[36] and a glass transition temperature of 5 °C. An approximately 1 μm thick film of ePP was prepared by drop casting a 5 mg/mL ePP solution in decaline onto a NaCl crystal. The dried film was floated onto a water surface and transferred onto a slotted silicon substrate, as shown in Figure 4a. NaCl residues were removed with distilled water. The film was stepwise stretched in the *y*-direction to a maximum strain of $\varepsilon = 61\%$. Afterward, the strain was stepwise reduced to $\varepsilon = 27\%$, where ε is the global strain in the *y*-direction given by $\varepsilon = (L - L_0)/L_0$, where L is the slit width and $L_0 = 150\ \mu$m is the initial slit width. To prevent damage to the tip and film, the SFM tip was retracted while varying the strain. After each stretching step, the same area of the free-standing polymer film was imaged with tapping mode SFM, as described previously.[51] To correct for global displacements of the specimen, the series of images was registered by laterally shifting individual images to achieve a best fit. Angles and lamella lengths were measured using ImageJ.[52] The relative elongation $(l - l_0)/l_0$ of the individual lamellae was calculated from the initial length l_0 of the lamellae and their length l at global strain ε.

Figure 5a shows the deformations of a two-dimensional quadrilateral upon uniaxial elongation along its diagonal. The deformation of the left-hand side of the quadrilateral is shown in Figure 5b,c. The relations between the initial length of the side l_0 and the lengths a and b and its length l at strain ε and the lengths a and $b(1 + \varepsilon)$ are given by the Pythagorean formula. From this, the relative elongation of a side of the quadrilateral is calculated to be

$$(l - l_0)/l_0 = [1+2\varepsilon(1+\varepsilon/2)\sin^2(\alpha_0)]^{1/2}$$

The angle α_0 is defined in Figure 5. The relation between the angle $(\alpha + \beta)$ at strain ε and the initial angle $(\alpha_0 + \beta_0)$ at strain $\varepsilon = 0$ can be easily derived from the geometric relations given in Figure 5.

Acknowledgment. We thank N. Rehse and M. Jecke for their contributions to the design of the setup and sample preparation. We thank B. Rieger for providing the ePP, G. Schröder-Turk and M. Neumann for useful discussions, and S. McGee for proofreading the manuscript. This work was supported by the Volkswagen Foundation and the Deutsche Forschungsgemeinschaft. Author contributions: R.M. designed the experiment together with N. Rehse and M. Jecke. M.F. performed the experiments and analyzed the data. M.F. and R.M. jointly interpreted the results and wrote the paper.

Supporting Information Available: Movie showing an animated series of SFM phase images upon stretching the ePP film from $\varepsilon = 0\%$ to $\varepsilon = 61\%$. In the movie, the image sequence has been added in reversed order after the maximum strain is reached. This facilitates observing the details of the micromechanics, while watching the movie in a continuous loop. Only every tenth image of the entire series is shown in the movie. This material is available free of charge *via* the Internet at http://pubs.acs.org.

REFERENCES AND NOTES

1. Lakes, R. Foam Structures with a Negative Poisson's Ratio. *Science* **1987**, *235*, 1038–1040.
2. Evans, K. E.; Nkansah, M. A.; Hutchinson, I. J.; Rogers, S. C. Molecular Network Design. *Nature* **1991**, *353*, 124.
3. Evans, K. E. Auxetic Polymers: A New Range of Materials. *Endeavour, New Series* **1991**, *15*, 170–174.
4. Evans, K. E.; Alderson, A. Auxetic Materials: Functional Materials and Structures from Lateral Thinking!. *Adv. Mater.* **2000**, *12*, 617–628.
5. Yang, W.; Li, Z.-M.; Shi, W.; Xie, B.-H.; Yang, M.-B. On Auxetic Materials. *J. Mat. Sci.* **2004**, *39*, 3269–3279.
6. Liu, Y. P.; Hu, H. A Review on Auxetic Structures and Polymeric Materials. *Sci. Res. Essays* **2010**, *5*, 1052–1063.
7. Wojciechowski, K. W. Constant Thermodynamic Tension Monte Carlo Studies of Elastic Properties of a Two-Dimensional System of Hard Cyclic Hexamers. *Mol. Phys.* **1987**, *61*, 1247–1258.
8. Wojciechowski, K. W. Two-Dimensional Isotropic System with a Negative Poisson Ratio. *Phys. Lett. A* **1989**, *137*, 60–64.

9. Wojciechowski, K. W. Non-Chiral, Molecular Model of Negative Poisson Ratio in Two Dimensions. *J. Phys. A: Math. Gen.* **2003**, *36*, 11765–11778.
10. Rothenburg, L.; Berlin, A. A.; Bathurst, R. J. Microstructure of Isotropic Materials with Negative Poisson Ratio. *Nature* **1991**, *354*, 470–472.
11. Masters, I. G.; Evans, K. E. Models for the Elastic Deformation of Honeycombs. *Compos. Struct.* **1996**, *35*, 403–422.
12. Grima, J. N.; Farrugia, P. S.; Caruana, C.; Gatt, R.; Attard, D. Auxetic Behaviour from Stretching Connected Squares. *J. Mater. Sci.* **2008**, *43*, 5962.
13. Prall, D.; Lakes, R. S. Properties of a Chiral Honeycomb with a Poisson's Ratio of −1. *Int. J. Mech. Sci.* **1997**, *39*, 305–314.
14. Alderson, A.; Alderson, K. L.; Attard, D.; Evans, K. E.; Gatt, R.; Grima, J. N.; Miller, W.; Ravirala, N.; Smith, C. W.; Zied, K. Elastic Constants of 3-, 4- and 6-Connected Chiral and Anti-Chiral Honeycombs Subject to Uniaxial In-Plane Loading. *Compos. Sci. Technol.* **2010**, *70*, 1042–1048.
15. Grima, J. N.; Evans, K. E. Auxetic Behavior from Rotating Squares. *J. Mater. Sci. Lett.* **2000**, *19*, 1563–1565.
16. Grima, J. N.; Gatt, R.; Ravirala, N.; Alderson, A.; Evans, K. E. Negative Poisson's Ratios in Cellular Foam Materials. *Mater. Sci. Eng., A* **2006**, *423*, 214–218.
17. Grima, J. N.; Gatt, R.; Alderson, A.; Evans, K. E. An Alternative Explanation for the Negative Poisson's Ratios in α-Cristobalite. *Mater. Sci. Eng., A* **2006**, *423*, 219–224.
18. Bianchi, M.; Scarpa, F.; Banse, M.; Smith, C. W. Novel Generation of Auxetic Open Cell Foams for Curved and Arbitrary Shapes. *Acta Mater.* **2001**, *59*, 686–691.
19. Grima, J. N.; Attard, D.; Gatt, R.; Cassar, R. N. A Novel Process for the Manufacture of Auxetic Foams and for their Re-Conversion to Conventional Form. *Adv. Eng. Mater.* **2009**, *11*, 533–535.
20. Caddock, B. D.; Evans, K. E. Microporous Materials with Negative Poisson's Ratios. I. Microstructure and Mechanical Properties. *J. Phys. D: Appl. Phys.* **1989**, *22*, 1877–1882.
21. Alderson, K. L.; Webber, R. S.; Kettle, A. P.; Evans, K. E. Novel Fabrication Route for Auxetic Polyethylene. Part 1. Processing and Microstructure. *Polym. Eng. Sci.* **2005**, *45*, 568–578.
22. Ravirala, N.; Alderson, A.; Alderson, K. L.; Davies, P. J. Auxetic Polypropylene Films. *Polym. Eng. Sci.* **2005**, *45*, 517–528.
23. Pickles, A. P.; Alderson, K. L.; Evans, K. E. The Effects of Powder Morphology on the Processing of Auxetic Polypropylene (PP of Negative Poisson's Ratio). *Polym. Eng. Sci.* **1996**, *36*, 636–642.
24. Alderson, K. L.; Alderson, A.; Smart, G.; Simkins, V. R.; Davies, P. J. Auxetic Polypropylene Fibres Part 1—Manufacture and Characterisation. *Plast., Rubber Compos.* **2002**, *31*, 344–349.
25. Grima, J. N.; Gatt, R. Perforated Sheets Exhibiting Negative Poisson's Ratios. *Adv. Eng. Mater.* **2010**, *12*, 460–464.
26. Bertoldi, K.; Reis, P. M.; Willshaw, S.; Mullin, T. Negative Poisson's Ratio Behavior Induced by an Elastic Instability. *Adv. Mater.* **2010**, *22*, 361–366.
27. Nielsen, L. E.; Landel, R. F. *Mechanical Properties of Polymers and Composites*, 2nd ed.; Marcel Dekker: New York, 1994; Vol. 90.
28. Aboulfaraj, M.; G'Sell, C.; Ulrich, B.; Dahoun, A. *In Situ* Observation of the Plastic Deformation of Polypropylene Spherulites Under Uniaxial Tension and Simple Shear in the Scanning Electron Microscope. *Polymer* **1995**, *36*, 731–742.
29. Hild, S.; Gutmannsbauer, W.; Lüthi, R.; Fuhrmann, J.; Güntherodt, H.-J. A Nanoscopic View of Structure and Deformation of Hard Elastic Polypropylene with Scanning Force Microscopy. *J. Polym. Sci., Part B: Polym. Phys.* **1996**, *34*, 1953–1959.
30. Hild, S.; Rosa, A.; Marti, O., Deformation Induced Changes in Surface Properties of Polymers Investigated by Scanning Force Microscopy. In *Scanning Probe Microscopy of Polymers*; Ratner, B. D.; Tsukruk, V. V., Eds.; American Chemical Society: Washington, DC, 1998; pp 110−129.
31. Petermann, J.; Ebener, H. On the Micromechanisms of Plastic Deformation in Semicrystalline Polymers. *J. Macromol. Sci. Part B Phys.* **1999**, *5&6*, 837–846.
32. Godehardt, R.; Rudolph, S.; Lebek, W.; Goerlitz, S.; Adhikari, R.; Allert, E.; Giesemann, J.; Michler, G. H. Morphology and Micromechanical Behavior of Blends of Ethene/1-Hexene Copolymers. *J. Macromol. Sci. Part B Phys.* **1999**, *38*, 817–835.
33. Kravchenko, R. L.; Sauer, B. B.; McLean, R. S.; Keating, M. Y.; Cotts, P. M.; Kim, Y. H. Morphology Investigation of Stereoblock Polypropylene Elastomer. *Macromolecules* **2000**, *33*, 11–13.
34. Auriemma, F.; De Rosa, C. Stretching Isotactic Polypropylene: From "Cross-α" to Crosshatches, from γ-Form to α-Form. *Macromolecules* **2006**, *39*, 7635–7647.
35. Auriemma, F.; De Rosa, C.; Corradi, M. Stereoblock Polypropylene as a Prototype Example of Elasticity *via* a Flip-Flop Reorientation of Crystals in a Compliant Matrix. *Adv. Mater.* **2007**, *19*, 871–874.
36. Boger, A.; Heise, B.; Troll, C.; Marti, O.; Rieger, B. Orientation of the α- and γ-Modification of Elastic Polypropylene at Uniaxial Stretching. *Eur. Polym. J.* **2007**, *43*, 3573–3586.
37. Nozue, Y.; Shinohara, Y.; Ogawa, Y.; Sakurai, T.; Hori, H.; Kasehara, T.; Yamaguchi, N.; Yagi, N.; Amemiya, Y. Deformation Behavior of Isotactic Polypropylene Spherulite During Hot Drawing Investigated by Simultaneous Microbeam SAXS-WAXS and POM Measurement. *Macromolecules* **2007**, *40*, 2036–2045.
38. Thomas, C.; Ferreiro, V.; Coulon, G.; Seguela, R. *In Situ* AFM Investigation of Crazing in Polybutene Spherulites Under Tensile Drawing. *Polymer* **2007**, *48*, 6041–6048.
39. Hobbs, J. K.; Winkel, A. K.; McMaster, T. J.; Humphris, A. D. L.; Baker, A. A.; Blakely, S.; Aissaoui, M.; Miles, M. J. Some Recent Developments in SPM of Crystalline Polymers. *Macromol. Symp.* **2001**, *167*, 1–14.
40. Dietrich, U.; Hackmann, M.; Rieger, B.; Klinga, M.; Leskelä, M. Control of Stereoerror Formation with High-Activity "Dual-Side" Zirconocene Catalysts: A Novel Strategy to Design the Properties of Thermoplastic Elastic Polypropylenes. *J. Am. Chem. Soc.* **1999**, *121*, 4348–4355.
41. Rehse, N.; Marr, S.; Scherdel, S.; Magerle, R. Three-Dimensional Imaging of Semicrystalline Polypropylene with 10 nm Resolution. *Adv. Mater.* **2005**, *17*, 2203–2206.
42. Lotz, B.; Wittmann, J. C.; Lovinger, A. J. Structure and Morphology of Poly(propylenes): A Molecular Analysis. *Polymer* **1996**, *37*, 4979–4992.
43. Norton, D. R.; Keller, A. The Spherulitic and Lamellar Morphology of Melt-Crystallized Isotactic Polypropylene. *Polymer* **1985**, *26*, 704–716.
44. Schönherr, H.; Wiyatno, W.; Pople, J.; Frank, C. W.; Fuller, G. G.; Gast, A. P.; Waymouth, R. M. Morphology of Thermoplastic Elastomers: Elastomeric Polypropylene. *Macromolecules* **2002**, *35*, 2654–2666.
45. Sawatari, C.; Matsuo, M. Elastic Modulus of Isotactic Polypropylene in the Crystal Chain Direction as Measured by X-Ray Diffraction. *Macromolecules* **1986**, *19*, 2653–2656.
46. Carlson, E. D.; Fuller, G. G.; Waymouth, R. M. Transient Birefringence of Elastomeric Polypropylene Subjected to Step Shear Strain. *Macromolecules* **1999**, *32*, 8094.
47. Wiyatno, W.; Pople, J. A.; Gast, A. P.; Waymouth, R. M.; Fuller, G. G. Dynamic Response of Stereoblock Elastomeric Polypropylene Studied by Rheooptics and X-Ray Scattering. 2. Orthogonally Oriented Crystalline Chains. *Macromolecules* **2002**, *35*, 8498.
48. Ovchinnikov, V. A.; Zhorov, V. A.; Baskaev, Z. P. Elasticity of the Crystal Lattice of Polyethylene Terephthalate. *Mekhanika Polimerov* **1972**, *6*, 982–986.
49. Strobl, G. From the Melt *via* Mesomorphic and Granular Crystalline Layers to Lamellar Crystallites: A Major Route Followed in Polymer Crystallization?. *Eur. Phys. J. E* **2000**, *3*, 165–183.
50. Sirota, E. B. Polymer Crystallization: Metastable Mesophases and Morphology. *Macromolecules* **2007**, *40*, 1043–1048.
51. Dietz, C.; Zerson, M.; Riesch, C.; Franke, M.; Magerle, R. Surface Properties of Elastomeric Polypropylenes Studied with Atomic Force Microscopy. *Macromolecules* **2008**, *41*, 9259–9266.
52. Abramoff, M. D.; Magelhaes, P. J.; Ram, S. J. Image Processing with ImageJ. *Biophotonics Int.* **2004**, *11*, 36–42.